**PAPER**

Check for updates

Feasibility of the reaction between (R)-3-hydroxybutyrate & hydroxyl radicals

Peter A. C. McPherson, [ID] *[a] Ruaidhrí MacDonnell[b] and Ben M. Johnston[c]

Energetic particles and secondary radiation encountered by astronauts during space flight result in the formation of a range of reactive oxygen species, including hydroxyl radicals (HO$^\bullet$), which can lead to premature cell death. Several strategies have been proposed to combat the intracellular effects of radiation including use of exogeneous antioxidants. We have investigated the reaction between the major ketone body (R)-3-hydroxybutyrate (HB$^-$) and HO$^\bullet$ at the SMD/M062X/6-311++G(d,p) level of theory. This revealed a bimolecular rate constant of 6.20×10^9 dm^3 mol^{-1} s^{-1} with hydrogen atom abstraction at the hydroxyalkyl C–H bond constituting the predominate reaction channel ($\Gamma \approx 30\%$). Proton coupled electron transfer between the hydroxyl group and HO$^\bullet$ was thermodynamically and kinetically the least favourable ($k = 8.20 \times 10^7$ dm^3 mol^{-1} s^{-1}, $\Gamma \approx 1.3\%$) but produced an oxygen-centred radical exhibiting SOMO–HOMO inversion. Hydrogen abstraction at the methylene ($k \approx 1 \times 10^9$ dm^3 mol^{-1} s^{-1}, $\Gamma \approx 20\%$) and methyl ($k \approx 6 \times 10^8$ dm^3 mol^{-1} s^{-1}, $\Gamma \approx 10\%$) sites was of intermediate reactivity. Our estimates show that in dietary ketosis the half-life of HO$^\bullet$ is shorter on reaction with HB$^-$ than ascorbate ($t_{\frac{1}{2}} = 3.73 \times 10^{-8}$ *vs.* 4.81×10^{-7} s) suggesting that this is a viable approach for reducing the cellular impact of ionising radiation.

Introduction

Modelling the radiation environment beyond low-Earth orbit presents a significant challenge due to the complex nature of the galactic cosmic radiation (GCR).[1] This is of particular relevance as we explore the potential for human missions to Mars, during which astronauts are likely to be exposed to GCR in excess of 0.1 Sv h^{-1}.[2,3] While high energy electromagnetic radiation and spallation products can directly ionise biological molecules, a major pathway of cell damage is radiolysis of cellular water and formation of hydroxyl radicals (HO$^\bullet$).[4,5] The radiochemical yield (G) for HO$^\bullet$ from the reaction

$$H_2O \rightsquigarrow e_{aq}^-, H^\bullet, HO^\bullet, H_2, H_2O_2, H_3O^+ \qquad (1)$$
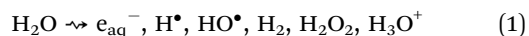
is *ca.* 2.4, which in our context is equivalent to almost 25 nmol dm^3 h^{-1}. The hydroxyl radicals so-formed are potent electrophiles and the most reactive of the oxygen-centred radicals, indiscriminately oxidising biological molecules,[6] leading to (*inter alia*) corneal opacification and hereditary radiation damage. It follows that exploring strategies to reduce cellular free radical flux is of relevance not only to surviving in the space

radiation environment,[7] but other areas where the impact of ionising radiation on humans needs to be minimised.

Reducing the formation of free radicals *in vivo* can involve the use of antioxidants which function in a range of ways.[8] At a global level, the characteristics of the frontier molecular orbitals can provide crude insights into the reactivity of the antioxidant through the use of conceptual density functional theory.[9] However, a more comprehensive understanding can only be obtained from a consideration of the potential mechanisms involved.[10] Arguably the most fundamental antioxidant mechanism is single electron transfer (SET) from the electron donor (AH) to the acceptor (HO$^\bullet$) *via* electron tunnelling:

$$AH + HO^\bullet \rightarrow AH^{\bullet+} + HO^- \qquad (2)$$
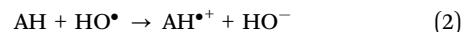
This process is clearly favoured when the electron donor has a low ionisation potential (IP) and the acceptor has a high electron affinity (EA).[11] The second major class of antioxidant mechanism is hydrogen abstraction, which can occur in several ways, but with the same overall stoichiometric result:

$$AH + HO^\bullet \rightarrow A^\bullet + H_2O \qquad (3)$$
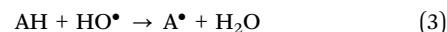
The first case is described as hydrogen atom transfer (HAT) and is characterised by the movement of the proton and electron to the same atomic orbital in the free radical. It follows that the feasibility of this process can be inferred from the bond dissociation energy (BDE) of the A–H bond.[12] A second process, proton-coupled electron transfer (PCET), is characterised by the

[a] School of Pharmacy & Pharmaceutical Science, Ulster University, Cromore Road, Coleraine BT52 1SA, UK. E-mail: p.mcpherson@ulster.ac.uk
[b] Faculty of Science, Technology, Engineering & Mathematics, The Open University, Milton Keynes MK7 6AA, UK
[c] Centre for Applied Science, Belfast Metropolitan College, Titanic Quarter Campus, Belfast BT3 9DT, UK

movement of a proton and electron from different orbitals on the donor to different orbitals on the acceptor *via* a compact hydrogen bonded pre-reaction complex.[13] This process cannot be distinguished from HAT by simple thermodynamic calculations; instead, a consideration of the transition state or the degree of electronic nonadiabaticity should be used. Alternatively, a separated proton and electron can tunnel to the product state in a concerted electron-proton transfer (CEPT) where no intermediate is involved.[14] Other processes described in the literature, *viz.* sequential electron transfer proton transfer (SETPT) and sequential proton loss electron transfer (SPLET), differ in the sequence that the protons/electrons are transferred.

On the issue of human exposure to GCR, an obvious solution would be to utilize an antioxidant cocktail,[15] but this presents the question of drug stability in space,[16] plus the consequences of an additional payload for longer missions. An alternative eluded to in the literature is to induce dietary ketosis.[17] Ketosis refers to the physiological state in which the concentration of the ketone bodies, *viz.* acetoacetic acid (pK_a = 3.58) and (*R*)-3-hydroxybutyric acid (pK_a = 4.41)† (Scheme S1), reach millimolar levels in response to reduced intracellular glucose availability.[18] The utility of ketosis in situations of high oxidative stress has been discussed elsewhere.[19]

In dietary ketosis, (*R*)-3-hydroxybutyrate (HB⁻) is the major circulating ketone body, rising to *ca.* 3 mmol dm⁻³, and is therefore a potential candidate for free radical scavenging.[20] An early precedent for this hypothesis was established in 1904 when Holleman demonstrated that pyruvate (the anion of an α-keto acid) reacts with hydrogen peroxide, a recognised reactive oxygen species.[21] Later, Haces *et al.* demonstrated that HB⁻ directly quenches HO•, and that HB⁻ can reduce lipid peroxidation in rat hippocampus.[22] Similar reactions have been observed with pyruvate,[23] lactate[24] and acetone,[25] with the latter itself considered a ketone body.

We have explored the thermodynamics and kinetics of the reaction between HB⁻ and HO• in the aqueous environment using the M06-2X density functional, which has previously been shown to be a satisfactory compromise between computational speed and accuracy.[26] In addition to exploring the title reaction, we have also drawn attention to some pitfalls associated with using approximations to deduce common reactivity indices.

Computational methods

All structures were prepared using the molecular editing program Avogadro[27] and all density functional calculations were performed using the electronic structure package Orca (Version 6.0).[28] Structures were optimized using the M06-2X functional[29] and 6-311++G(d,p) basis set,[30] using the RIJCOSX approximation with an auxiliary basis set to reduce computational time.[31] The D3 dispersion correction was employed in all calculations.[32] Unrestricted calculations were used for all open-shell species and local minima were confirmed by the absence of any imaginary modes. Zero-point energies and thermal corrections at 298 K

were included for calculation of energies and vibrational frequencies were scaled by a factor of 0.970 to correct for anharmonic behaviour.[32] For modelling reactions in the solvent phase, Truhlar's universal solvation model density (SMD) was used.[33] For the hydroxyl radical/anion pair, we followed the convention that the first solvation shell contains four explicit water molecules.[34] Formal reaction mechanisms were explored by establishing the minimum energy path between reactants and products using the nudged elastic band method as implemented in Orca.[35] Transition states were identified by the presence of a single imaginary mode corresponding to the expected motion along the reaction coordinate.

The thermal rate constant, k_T, was evaluated using transition state theory by way of the Eyring equation

$$k_T = \kappa(T)\sigma\left(\frac{k_B T}{h}\right)\exp\left(-\frac{\Delta G^\ddagger}{RT}\right) \quad (4)$$

in which $\kappa(T)$ is the Eckart tunnelling coefficient,[36,37] σ is the reaction path degeneracy,[38] k_B is the Boltzmann constant (1.38×10^{-26} kJ K⁻¹), T is temperature (298.15 K), h is the Planck constant (6.34×10^{-37} kJ s), R is the gas constant (8.314×10^{-3} kJ K⁻¹ mol⁻¹) and $\Delta G^\ddagger$ is the Gibbs activation energy which has been corrected for the 1 mol dm⁻³ standard state and solvent cage effects (= $\Delta G^{1atm} - 18.58$ kJ mol⁻¹ for a bimolecular reaction).[39]

As reactions involving HO• often occur at the limit of diffusion, the Smoluchowski rate constant, k_d,[40] was also evaluated using the relationship

$$k_d = 4\pi r_{AD}\left(\frac{k_B T}{6\pi\eta}\right)\left(\frac{1}{r_A} + \frac{1}{r_D}\right)N_A \quad (5)$$

where r_{AD} was taken as the sum of the radii of the reactants (for electron transfer), or the distance between the two participating atoms in the transition state (hydrogen transfer); r_A and r_D are the hydrodynamic radii of the acceptor (HO•) and donor (HB⁻) (see Table S2), respectively; η is the solvent viscosity (0.89 kJ s m⁻³ for water) and N_A is the Avogadro constant (6.02×10^{23} mol⁻¹). Finally, the diffusion-adjusted rate constant (k_n) was obtained using the Collins–Kimball theory,[41] where n is an index corresponding to the reaction under study, *i.e.*

$$k_n = \frac{k_T k_d}{k_T + k_d} \quad (6)$$

Results & discussion

In the aqueous environment at pH 7.4, (*R*)-3-hydroxybutyric acid (K_a = 1.99×10^{-5}) is virtually fully dissociated to the corresponding anion, (*R*)-3-hydroxybutyrate (HB⁻); the molar fraction of the anion is 0.9980 (see Fig. S1). Therefore, for this study, only the anion will be considered. A relaxed potential energy scan of HB⁻ was performed by rotation of the dihedral angle formed by H9–C2–C3–H10 in increments of 10°. This revealed two low-energy conformers with C_2 symmetry, but with the lowest energy species benefiting from a modest positive *gauche* effect (ϕ = 60.3°) due to an intermolecular hydrogen

---

† IUPAC names: 3-oxobutanoic acid and (*R*)-3-hydroxybutanoic acid.

This journal is © the Owner Societies 2025

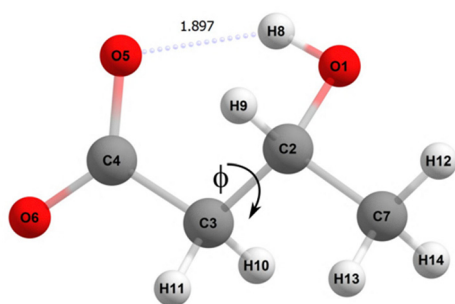*Phys. Chem. Chem. Phys.*, 2025, **27**, 20484–20492 | **20485**

Fig. 1 Optimised structure and atomic numbering scheme for (R)-3-hydroxybutyrate at the SMD/M06-2X/6-311++G level of theory.

bond, O8···H5 (1.897 Å) (Fig. 1). Similar structural arrangements have been previously observed in α-hydroxy acids in aqueous solution.[42] Only this lowest energy conformer is considered further in this work.

In principle, the reaction between HB^- and $HO^\bullet$ can occur in two main ways: single electron transfer and hydrogen abstraction, with the latter potentially involving hydrogen atom transfer, proton-coupled electron transfer, concerted electron-proton transfer, sequential electron transfer proton transfer or sequential proton loss electron transfer. As HB^- contains only saturated (C–C) bonds, radical adduct formation is unlikely. Likewise, with the possible exception of the hydroxyl group, the methylene or methyl carbons will not undergo proton transfer, and so we anticipate that hydrogen atom transfer will be the predominate process. To gain a crude overview of these processes, a series of common thermodynamic parameters (viz. ionisation potential, proton dissociation enthalpy, proton affinity and electron transfer enthalpy) were evaluated.[43] The results (Table S2) verified our initial conjecture that hydrogen atom transfer would be the predominate mechanism vs. other processes such as SETPT and SPLET.

Potential for electron transfer

As the reduction potential for HB^- is ca. −0.349 V at pH 7.0,[44] it is reasonable to expect the anion to donate electrons. Our first evaluation of this comes from the HOMO electron density (Fig. 2A), which is relatively delocalised across the anion with major contributions from the p-orbitals of O6 and C4. However, as has been discussed elsewhere,[45] the HOMO is not necessarily a reliable indicator of reactivity as the most available electrons may sit in other orbitals. An attempt to improve this

description was provided by Sjoberg and co-workers who introduced the concept of average local ionisation energy (ALIE).[46] In this formalism, the ALIE is taken as the average energy required to remove an electron from the species taking into account contributions from all orbitals. The ALIE for HB^- was evaluated[47] and is presented as a colour-mapped isosurface (Fig. 2B) from which we note that the ALIE surface is relatively homogeneous, indicating no sharply localized regions of low ionisation energy. However, the electrons surrounding the carboxylate group exhibit slightly lower ALIE (as indicated by the red-to-white gradient), suggesting that this region may be marginally more prone to electron donation. This observation is consistent with carboxylate's role as an electron-rich, anionic site, and may contribute to initial interactions with electrophilic species such as the hydroxyl radical. A final view is obtained from the isosurface obtained for the condensed Fukui function for electrophilic attack.[48] In Fig. 2C we see that O6 emerges as the main electron donor site, as indicated by the local maximum in the condensed Fukui function (blue region). We can reasonably expect that if single electron transfer occurs, it will be from the non-bonding orbital on O6 to the radical acceptor species.

Another common approach for assessing the potential for electron transfer draws from second-order perturbation theory, where a small HOMO–LUMO gap is often taken as indicative of chemical reactivity. In this context, Koopmans' approximation (more rigorously formalized under the Perdew–Levy theorem)[49] is used, such that the vertical ionisation potential (VIP) is taken as $-E_{HOMO}$ and electron affinity (EA) as $-E_{LUMO}$. While convenient, this approach is fundamentally limited when applied within the formalism of DFT. Specifically, the DFT Kohn–Sham orbitals are not true molecular orbitals, but rather mathematical constructs designed to reproduce the total electronic density of the system.[50] As a result, orbital energies, particularly for unoccupied states, can deviate significantly from the real system. This is clearly demonstrated in Table 1, where values for the well-characterized antioxidants ascorbate (Asc^-) and Trolox are included for comparison. Overall, we see that in all cases, the HOMO-derived VIP are substantially larger than those calculated as the total energy difference (i.e. $XH \rightarrow XH^\bullet + e^-$). When compared to Asc^- and Trolox, HB^- appears less likely to engage in electron transfer than these benchmark antioxidants.

Significantly, Table 1 emphasises the disparity between VIP estimated as $-E_{HOMO}$ and that calculated from the total energy difference. For example, comparing the energy-based VIP of
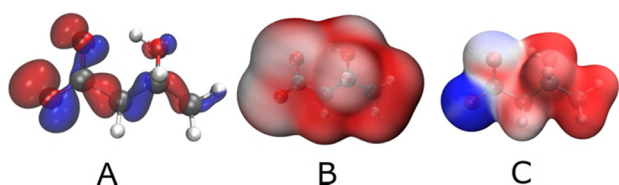

Fig. 2 (A) HOMO, (B) average local ionisation energy (ALIE) and (C) condensed Fukui (f^-) function for (R)-3-hydroxybutyrate. For (B) and (C) the colour progression from red to white to blue indicates increasing electron density.

Table 1 Vertical ionisation potential (I and VIP, kJ mol^{-1}) and electron affinity (A and EA, kJ mol^{-1}) for hydroxybutyrate (HB^-), ascorbate (Asc^-) and Trolox calculated at the SMD/M06-2X/6-311++G level of theory

	I $(-E_{HOMO})$	A $(-E_{LUMO})$	VIP^a	EA^b
HB^-	809.5	−24.9	546.9	−101.9
Asc^-	613.5	−12.6	392.5	−232.7
Trolox	679.8	−8.2	458.3	−131.7

^{a} Calculated as: $E(AH^\bullet) + E(e^-) - E(AH)$. ^{b} Calculated as: $E(AH^-) + E(e^-) - E(AH^{2-})$.

20486 | Phys. Chem. Chem. Phys., 2025, 27, 20484–20492

This journal is © the Owner Societies 2025

Asc$^-$ (392.5 kJ mol^{-1}) with its experimental value (371.47 kJ mol^{-1})[51] shows much better agreement *vs.* comparison with $-E_{HOMO}$ (809.46 kJ mol^{-1}). The discrepancy between the experimental value and that obtained from the total energy difference can be attributed to the inherent limitations of DFT – for example, errors in electron correlation. It is also worthwhile to note that some experimental IPs may relate more closely to adiabatic conditions. VIPs can only be reliably measured using fast techniques, such as low-temperature photoelectron spectroscopy, where the electron is ejected so rapidly that the nuclei do not have time to relax.[52] From this preceding discussion, we conclude that estimating VIP and EA from Kohn–Sham orbital energies is to be discouraged in all but the most rudimentary of work, or for large systems where computational costs are prohibitive.

Feasibility & kinetics of electron transfer

Given that some electron transfer from HB$^-$ is likely, the feasibility and kinetics of the process was investigated more fully. In general we consider electron transfer between a donor (HB$^-$) and acceptor (HO$^\bullet$) to occur so rapidly that there is insufficient time for geometry relaxation (the Frank–Condon principle). This concept was explored fully by Marcus and co-workers[53] who went on to demonstrate that for outer-sphere electron transfer, the thermal barrier height ($\Delta G^\ddagger$) can be evaluated using simple geometric arguments that yield:

$$\Delta G^\ddagger = \frac{(\lambda + \Delta G^\circ)^2}{4\lambda} \qquad (7)$$

In this expression, λ is the system reorganisation energy associated with the nuclear rearrangement required for formation of products (λ_i) and that of the surrounding solvent (λ_o), reasonably approximated by[54]

$$\lambda \approx \lambda_i + \lambda_o = \Delta E - \Delta G + \lambda_o \qquad (8a)$$

$$\lambda_o = (\Delta q)^2 \left(\frac{1}{\varepsilon_\infty} - \frac{1}{\varepsilon_o} \right) \left(\frac{1}{2r_A} + \frac{1}{2r_D} - \frac{1}{r_{AD}} \right) \qquad (8b)$$

where ΔE is the non-adiabatic energy difference between reactants and vertical products,[55] ΔG is the corrected standard Gibbs energy change, Δq is the amount of charge transferred, ε_∞ is the square of the index of refraction of the solvent (1.77 for water), ε_o is the dielectric constant of the solvent (78.40 for water), r_A and r_D are the radii of the acceptor and donor, respectively, and r_{AD} is the reaction distance (Table S3).[56] The result of eqn (7) is then substituted into the Eyring equation, assuming $\kappa(T) = 1$ for adiabatic processes, and adjusted by eqn (4) to obtain the rate constant for electron transfer (k_1).

Given the relatively large VIP and the qualitative impressions given by Fig. 2, we do not expect rapid electron transfer between HB$^-$ and HO$^\bullet$. Results (Table 2) support this view where we see that the electron transfer process is endergonic with $\Delta G = 27.33$ kJ mol^{-1} with a corresponding barrier height of $\Delta G^\ddagger = 43.08$ kJ mol^{-1}. While electron transfer can occur over relatively large distances (*ca.* 1 nm), in the case of HB$^-$ and HO$^\bullet$, this process is below the diffusion limit for these species ($k_1 = 1.76 \times 10^5$ *vs.*

Table 2 Non-adiabatic energy change (ΔE, kJ mol^{-1}), corrected Gibbs energy of reaction (ΔG, kJ mol^{-1}), system reorganisation energy (λ, kJ mol^{-1}), Gibbs energy of activation ($\Delta G^\ddagger$, kJ mol^{-1}), diffusion rate constant (k_d dm^3 mol^{-1} s^{-1}), SET rate constant (k_{SET}, dm^3 mol^{-1} s^{-1}) and apparent rate constant (k_1, dm^3 mol^{-1} s^{-1}) for electron transfer at 298.15 K

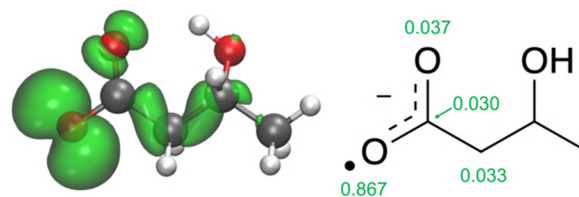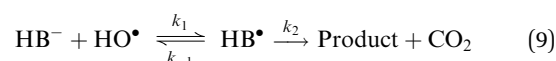| ΔE	ΔG	λ	$\Delta G^\ddagger$	k_d	k_{SET}	k_1
137.02	27.73	109.86	43.08	8.26×10^6	1.76×10^5	1.76×10^5

Fig. 3 Spin density of HB$^\bullet$ following electron transfer. Numerical values in green were obtained by Hirshfeld population analysis. The density isosurface was rendered at 0.05 a.u.

$k_d = 8.26 \times 10^6$ dm^3 mol^{-1} s^{-1}) and well below the rate of electron transfer between HO$^\bullet$ and Asc$^-$ at this level of theory (*ca.* 10^9 dm^3 mol^{-1} s^{-1}). However, as discussed elsewhere[57] endergonic electron transfer may still lead to a significant reaction channel if the product rapidly undergoes further reaction(s). With this in mind, we considered the reactivity of the HB$^\bullet$ so-formed in terms of its spin density (Fig. 3) from which we see that the electron transferred from O6 produces high spin density at this site in the radical product. This presents an opportunity for facile decarboxylation as has been previously established for similar structures.[58] This latter reaction is significantly exergonic ($\Delta G = -77.88$ kJ mol^{-1}) with a relatively small barrier height of $\Delta G^\ddagger = 3.61$ kJ mol^{-1}, giving $k_2 = 1.66 \times 10^9$ s^{-1}. However, as the reverse of the electron transfer process is exergonic, decarboxylation will be heavily dependent on the reaction conditions. Given that under physiological conditions the concentration of reactants is far below the standard one molar state, a steady-state approximation should be considered, *i.e.*

$$\text{HB}^- + \text{HO}^\bullet \underset{k_{-1}}{\overset{k_1}{\rightleftharpoons}} \text{HB}^\bullet \overset{k_2}{\longrightarrow} \text{Product} + \text{CO}_2 \qquad (9)$$

As $k_2 \gg k_{-1}$, the formation of HB$^\bullet$ is rate-limiting and the effective rate constant will be equal to k_1 (1.76×10^5 dm^3 mol^{-1} s^{-1}). While this is still not sufficient to compete with the reaction of HO$^\bullet$ with biological molecules, it is above the nominal threshold for a primary antioxidant suggested by Galano and Alvarez-Idaboy (1.18×10^3 dm^3 mol^{-1} s^{-1})[59] and will make a minor contribution to the overall radical scavenging ability of HB$^-$ (see later).

Hydrogen abstraction

It has previously been found that due to its relatively high Hartree–Fock component, the M06-2X functional can be associated with strong multireference character in hydrogen abstraction mechanisms.[60] To examine this, we used the T1 diagnostic

This journal is © the Owner Societies 2025

Phys. Chem. Chem. Phys., 2025, **27**, 20484–20492 | **20487**

for all reactants and transition states by evaluating the CCSD(T)/M06-2X/6-311G++(d,p) energies. For all cases, T1 < 0.045 (Table S4) and so we conclude that the performance of the M06-2X density functional is adequate for this study. Likewise, in all reactants and transition states, the deviation of $\langle S^2 \rangle$ from the eigenvalue $S(S + 1) = 0.75$ did not exceed 2%, although as it has been argued that as spin contamination is poorly defined for density functionals, alternative formalisms may be more appropriate.[61]

The abstraction of hydrogen atoms from HB$^-$ by HO$^\bullet$ is governed by the corresponding bond dissociation energy (BDE).[62] The trend in BDEs in Table 3 is largely as expected, except for the O1–H8 bond, which is slightly higher than the corresponding value in 2-butanol (84.84 kJ mol^{-1}) at the same level of theory. This is reflective of the intermolecular hydrogen bond which must be overcome in addition to the O1–H8 bond itself. The lowest BDE obtained at C2–H9 can be attributed to the electron-withdrawing inductive effect of the hydroxyl substituent. We also report the enthalpy and Gibbs energy of reaction which better describe the influence of the reacting radical on the energetics of the system. Of note is the case of O1–H8 which is endothermic ($\Delta H = 10.32$ kJ mol^{-1}) yet exergonic ($\Delta G = -49.11$ kJ mol^{-1}). Evans and Polanyi[63] demonstrated that for HAT processes, $|\Delta S| \approx 0$, and so for hydrogen abstraction at O1–H8, we surmise that PCET is a more likely mechanism as entropy is clearly a significant factor for this channel (due to solvent reorganisation). Hydrogen abstraction at all other sites is exothermic and exergonic.

As hydrogen abstraction in the HB$^-$ + HO$^\bullet$ system could occur in two main ways (*viz.* hydrogen atom transfer and proton-coupled electron transfer) it is necessary to examine the properties of each transition state. For all reactions, weakly-bound pre-reactive complexes were found in the entry channel. In each of these, the oxygen of HO$^\bullet$ approaches the hydrogen to be abstracted to form a hydrogen-bonded intermediate. The reaction then proceeds *via* a transition state (Fig. S2) through lengthening of the C–H bond (0.1136–0.1174 nm) and shortening of the HO$\cdots$H distance (0.1430–0.1650 nm). When the new HO–H bond forms, the products exist in a complex state until finally becoming separated as the final asymptotic products. Examining the charge (by natural population analysis),[64,65] Hirshfeld atomic spin density and natural 1S orbital occupancy of the transition states (Table 4) provides a good indication of the hydrogen abstraction mechanism. The hydrogen abstracted at O1–H8 has

Table 4 Natural population analysis charge, Hirshfeld atomic spin density and natural atomic orbital occupancy for the 1S orbital at the transition state for each potential hydrogen abstraction site

Bond	NPA charge	Hirshfeld ASD	1S occupancy
O1–H8	0.452	−0.001	0.544
C2–H9	0.203	0.020	0.796
C3–H10	0.239	0.024	0.760
C3–H11	0.245	0.024	0.755
C7–H12	0.226	0.027	0.773
C7–H13	0.231	0.027	0.769
C7–H14	0.253	0.031	0.746

clear proton character with a charge of *ca.* 0.5e and zero spin.[66] When this is considered along the minimum energy path (Fig. 4A), we see that the charge of H8 remains constant, while that of the donor and acceptor decrease and increase, respectively. Likewise, Fig. 4B shows that the spin of H8 remains constant while that of the donor and acceptor gradually switch. At the transition geometry (Fig. 4C), the HOMO density is spread over both HB$^-$ and HO$^\bullet$, forming a channel to mediate electron transfer (Fig. 4D). The SOMO of the transition state is orthogonal to the transition vector (Fig. 4E), which is indicative of PCET. Hydrogen abstraction from all remaining sites is more consistent with HAT, with the charge of the migrating hydrogen in the range 0.203–0.253e and 1S occupancy of 0.746–0.796.[67]

In general, hydrogen abstraction at O–H bonds would occur more rapidly than C–H bonds. Rate constants (Table 5) show the opposite – abstraction at O1–H8 is two orders of magnitude slower than at methylene carbons, in this case due to the stabilising effect of the intermolecular hydrogen bond. The large imaginary mode (-1899.76 cm^{-1}) associated with the O1$\cdots$H8$\cdots$OH transition vector is indicative of a compact transition state with significant tunnelling, which off sets the high barrier height to some extent.[68] Nevertheless, this reaction is below the diffusion limit and will constitute only a minor reaction channel. The highest rate constant is observed at C2–H9 and is likely due to
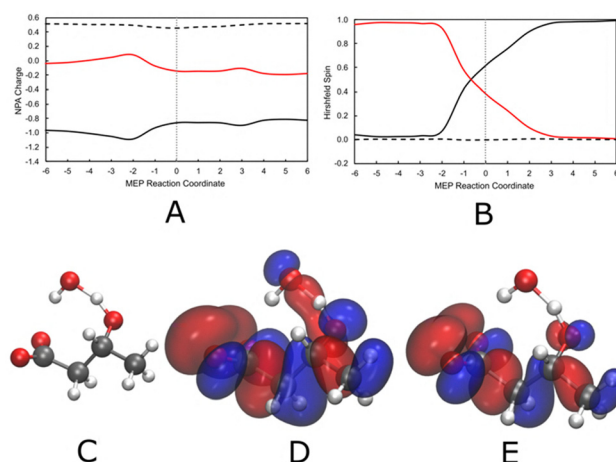

Fig. 4 (A) Change in NPA charge in acceptor (red), donor (black) and H7 (black dashed). (B) Change in Hirshfeld spin in acceptor (red), donor (black) and H7 (black dashed). (C) Transition state geometry for PCET. (D) HOMO and (E) SOMO density isosurfaces rendered at 0.05 a.u.

Table 3 Bond dissociation energy (BDE, kJ mol^{-1}), enthalpy ($\Delta_r H$, kJ mol^{-1}) and Gibbs energy of reaction for hydrogen abstraction ($\Delta_r G$, kJ mol^{-1}) at each reactive site in HB$^-$

Bond	BDE	$\Delta_r H$	$\Delta_r G$
O1–H8	393.47	10.32	−49.11
C2–H9	330.42	−52.73	−111.77
C3–H10	341.74	−41.40	−100.42
C3–H11	341.73	−41.42	−100.13
C7–H12	366.93	−16.21	−76.36
C7–H13	366.92	−16.23	−76.04
C7–H14	366.86	−16.29	−76.65

Table 5 Imaginary frequency (ν^*, cm^{-1}), Eckart tunnelling coefficient ($\kappa(T)$), Gibbs activation energy ($\Delta G^{\ddagger}$, kJ mol^{-1}), thermal rate constant (k_T, dm^3 mol^{-1} s^{-1}), diffusion-controlled rate constant (k_d, dm^3 mol^{-1} s^{-1}) and apparent rate constant (k_n, dm^3 mol^{-1} s^{-1}) for each reaction site in HB$^-$

Site	ν^*	$\kappa(T)$	$\Delta G^{\ddagger}$	k_T	k_d	k_n
O1–H8	−1899.76	19.07	55.19	9.17×10^7	7.90×10^8	8.21×10^7
C2–H9	−456.16	1.20	28.57	2.65×10^{11}	1.74×10^9	1.73×10^9
C3–H10	−817.25	1.63	39.76	3.95×10^9	1.80×10^9	1.24×10^9
C3–H11	−827.25	1.03	38.20	4.67×10^9	1.66×10^9	1.23×10^9
C7–H12	−834.93	1.81	41.63	2.06×10^9	8.88×10^8	6.20×10^8
C7–H13	−851.18	1.80	41.20	2.43×10^9	8.86×10^8	6.49×10^8
C7–H14	−848.20	1.64	40.92	2.48×10^9	8.89×10^8	6.55×10^8

hydrogen-bond-assisted activation due to the polarising effect of the adjacent hydroxyl group.[69] The imaginary mode for this channel is due to the asymmetric movement of the bridging hydrogen and is associated with a small degree of tunnelling, but overall the rate remains diffusion-limited. HAT at C3–H10 and C3–H11 likely benefits from a weak captodative effect; the electron withdrawing hydroxyl and the electron donating carboxyl would stabilise the transition state, lowering the energy barrier and increasing the rate. Finally, HAT at the methyl positions has an average rate constant of 6.4×10^8 dm^3 mol^{-1} s^{-1} which is similar to that previously obtained for the methyl position on valeric acid.[70]

HAT product radicals

When an antioxidant undergoes electron transfer *etc.*, it is transformed into a new radical species, which is often assumed to be innocuous, but this is not necessarily the case. In the presence of oxygen, carbon-centred radicals undergo rapid conversion to the corresponding peroxyl radical.[71] In the case of HAT at C2–H9 (the most thermodynamically and kinetically favoured channel) we would expect formation of an α-hydroxyalkylperoxyl radical, which would subsequently undergo an intermolecular hydrogen shift to eliminate HOO$^\bullet$,[72] in this case, yielding acetoacetate (Scheme S2). However, inspection of Fig. 5 shows that the radicals formed by hydrogen abstraction are distonic and therefore contain an internal oriented electric field. This confers a degree of stability (*vs.* radicals where the charge and spin are co-localised), which leads to the resultant species reacting more like an anion than a radical.[73] The oxygen-centred radical formed by PCET at O1–H8 is unusual in that the SOMO is submerged 0.1309 eV below the HOMO, violating the Aufbau principle. Such SOMO–HOMO inversion has previously been reported for 1-methylcytosine in which sequential one-electron oxidation produces a species with a stable triplet ground state.[74]

Overall kinetics

The overall bimolecular rate constant for the title reaction is $k = 6.20 \times 10^9$ dm^3 mol^{-1} s^{-1}, which is in keeping with experimental values obtained for similar reactions. For example, in a pulse radiolysis study, Neta *et al.* found that the reaction between HO$^\bullet$ and butyrate predominantly forms the secondary radical CH$_3$CH$_2\dot{C}$HCOO$^-$ with a rate constant in
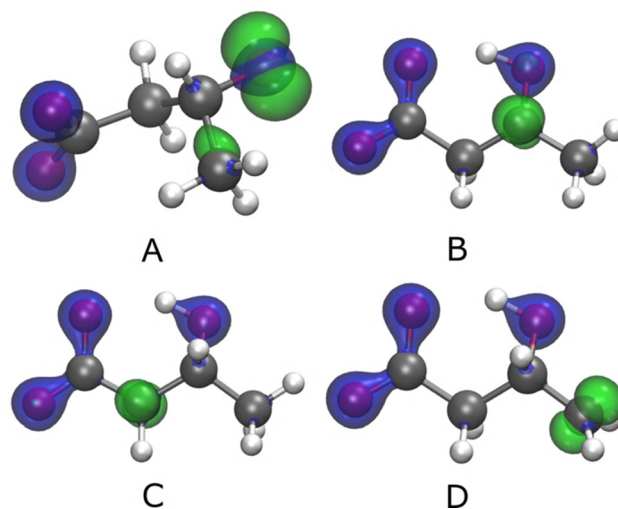

Fig. 5 (A) Distribution of charge (blue) and spin (green) in radicals formed by hydrogen abstraction. (A) PCET at O1–H8. (B) HAT at C2–H9. (C) HAT at C3–H10 (also representative of HAT at C3–H11). (D) HAT at C7–H12 (also representative of HAT at C7–H13 and C7–H14). The density isosurface was rendered at 0.3 a.u. (for charge) and 0.03 a.u. (for spin).

the region of 10^9 dm^3 mol^{-1} s^{-1}.[75] A summary of the rate constants for each reaction channel is provided in Table 6, together with branching ratios taken as

$$\Gamma = \frac{k_{\text{channel}}}{6.20 \times 10^9} \times 100 \tag{10}$$

where the denominator is the sum of all the rate constants listed in Table 6. As anticipated, SET makes a very minor contribution to the overall rate constant (0.1%), whereas HAT at C2–H9 contributes almost 30% to the overall value.

From a computational perspective, evaluation of the rate constants for the antioxidant-radical processes is convenient, but it does not take into account the underpinning pharmacology of these processes. Returning to our context of dietary ketosis, if we take [HB$^-$] $\approx$ 3 mmol dm^{-3}, then the half-life for the reaction with HO$^\bullet$ will be given by

$$t_{1/2} = \frac{\ln 2}{k[\text{HB}^-]} \tag{11}$$

which returns $t_{\frac{1}{2}} = 3.73 \times 10^{-8}$ s. For comparison, pharmacokinetic data shows that consumption of 1500 mg Vitamin C per day results in a serum concentration of *ca.* 200 μmol dm^{-3}.[76]

Table 6 Rate constants (k_n, dm^3 mol^{-1} s^{-1}) multiplied by the molar fraction of HB$^-$ present at pH 7.4, branching ratio (Γ, %) and dominant reaction mechanism for each reaction site in HB$^-$

Site	$k_n \times 0.998$	Γ	Mechanism
Anion	$k_1 = 8.24 \times 10^6$	0.1	SET
O1–H8	$k_3 = 8.20 \times 10^7$	1.3	PCET
C2–H9	$k_4 = 1.73 \times 10^9$	27.9	HAT
C3–H10	$k_5 = 1.24 \times 10^9$	19.9	HAT
C3–H11	$k_6 = 1.22 \times 10^9$	19.8	HAT
C7–H12	$k_7 = 6.19 \times 10^8$	10.0	HAT
C7–H13	$k_8 = 6.48 \times 10^8$	10.5	HAT
C7–H14	$k_9 = 6.53 \times 10^8$	10.5	HAT

This journal is © the Owner Societies 2025

Phys. Chem. Chem. Phys., 2025, **27**, 20484–20492 | **20489**

Taking $k = 7.2 \times 10^9$ dm^3 mol^{-1} s^{-1} for Asc$^-$ + HO$^\bullet$,[77] this gives $t_{\frac{1}{2}} = 4.81 \times 10^{-7}$ s. Accordingly, dietary ketosis seems like a viable strategy to reduce oxidative stress *in vivo*, and has the added benefit of not requiring the use of antioxidant supplements or pharmaceuticals.

Conclusions

Hydroxyl radicals are the proximal cause of much of the oxidative damage arising from exposure to ionising radiation. Due to the high rate of reaction of HO$^\bullet$ with biological molecules, antioxidants must be present at relatively high concentrations in order to be effective scavengers. In ketosis, (*R*)-3-hydroxybutyrate is present at millimolar concentrations and is capable of reacting with HO$^\bullet$ in two main ways: single electron transfer and hydrogen atom transfer, with abstraction of the H9 atom appearing to be the most thermodynamically and kinetically favourable ($\Gamma \approx 30\%$).

While this work provides an initial rationale for considering ketosis as one component of a broader radiation countermeasure strategy in prolonged spaceflight, it is important to recognise the complex biological context in which these reactions occur. In ketogenic states, shifts in redox balance, pH, and enzyme expression can influence both the concentration and reactivity of key species. Moreover, variability in ketone body distribution and clearance rates may affect the effective concentration of HB$^-$. Although these parameters are relatively well understood under terrestrial conditions (HB$^-$ production *ca.* 0.45 mmol dm^{-3} h^{-1}), they could be altered in low-gravity environments such as those encountered during space flight. Nevertheless, the relative ease of inducing ketosis, *e.g.* through dietary interventions, makes this a practical and potentially valuable strategy. Consideration, however, should be given to the systemic effects of sustained ketosis, including its impact on renal function and cognitive performance in astronauts.

Author contributions

PMcP conceptualization, methodology, investigation, writing – original draft preparation, formal analysis; RMacD: investigation, methodology; BMJ: investigation, methodology.

Conflicts of interest

There are no conflicts to declare.

Data availability

The data that support the findings of this study are available within the article and its SI. Supplementary information: Thermodynamics of hydrogen abstraction; hydrodynamic radii; T1 diagnostic; geometry, HOMO & SOMO of transition states; Cartesian coordinates for relevant structures. See DOI: **https://doi.org/10.1039/d5cp02665b**.

Detailed theoretical data that support the findings of this study are available from the corresponding author upon reasonable request.

Notes and references

1 J. C. Chancellor, R. S. Blue, K. A. Cengel, S. M. Auñón-Chancellor, K. H. Rubins, H. G. Katzgraber and A. R. Kennedy, *npj Microgravity*, 2018, **4**, 8.
2 G. Onorato, E. Di Schiavi and F. Di Cunto, *Front. Phys.*, 2020, **8**, 362.
3 M. I. Dobynde and Y. Y. Shprits, *Life Sci. Space Res.*, 2020, **24**, 116.
4 T. Christoudias, J. Kirkby, D. Stolzenburg, A. Pozzer, E. Sommer, G. P. Brasseur, M. Kulmala and J. Lelieveld, *Commun. Earth Environ.*, 2024, **5**, 326.
5 E. C. Ransdell-Green, J. Baranowska-Kortylewicz and D. Wang, *Antioxidants*, 2025, **14**, 79.
6 G. M. Chaban, D. Wang and W. M. Huo, *J. Phys. Chem. A*, 2015, **119**, 377–382.
7 M. Skirzewski and A. Skirzewski, *J. Neurochem.*, 2025, **169**, e16233.
8 G. Martemucci, C. Costagliola, M. Mariano, L. D'andrea, P. Napolitano and A. G. D'Alessandro, *Oxygen*, 2022, **2**, 48.
9 L. R. Domingo, M. Ríos-Gutiérrez and P. Pérez, *Molecules*, 2016, **21**, 748.
10 A. Galano, *J. Mex. Chem. Soc.*, 2015, **59**, 231–262.
11 A. Galano, *J. Phys. Chem. B*, 2007, **111**, 12898–12908.
12 H. Basch and S. Hoz, *J. Phys. Chem. A*, 1997, **101**, 4416–4431.
13 R. Tyburski, T. Liu, S. D. Glover and L. Hammarström, *J. Am. Chem. Soc.*, 2021, **143**, 560–576.
14 Y. Georgievskii and A. A. Stuchebrukhov, *J. Chem. Phys.*, 2000, **113**, 10438–10450.
15 C. A. Montesinos, R. Khalid, O. Cristea, J. S. Greenberger, M. W. Epperly, J. A. Lemon, D. R. Boreham, D. Popov, G. Gorthi, N. Ramkumar and J. A. Jones, *Life*, 2021, **11**, 829.
16 J. F. Reichard, S. E. Phelps, K. R. Lehnhardt, M. Young and B. D. Easter, *npj Microgravity*, 2023, **9**, 35.
17 N. D. Turner, L. A. Braby, J. Ford and J. R. Lupton, *Nutrition*, 2002, **18**, 904.
18 P. A. C. McPherson and J. McEneny, *J. Physiol. Biochem.*, 2012, **68**, 141.
19 A. Paoli, G. M. Tinsley, M. P. Mattson, I. De Vivo, R. Dhawan and T. Moro, *Trends Endocrinol. Metab.*, 2024, **35**, 125–141.
20 A. Julio-Amilpas, T. Montiel, E. Soto-Tinoco, C. Gerónimo-Olvera and L. Massieu, *J. Cereb. Blood Flow Metab.*, 2015, **35**, 851–860.
21 M. A. F. Holleman, *Recl. Trav. Chim. Pays-Bas Belg.*, 1904, **23**, 169–171.

20490 | *Phys. Chem. Chem. Phys.*, 2025, **27**, 20484–20492

This journal is © the Owner Societies 2025

22 M. L. Haces, K. Hernandez-Fonseca, O. N. Medina-Campos, T. Montiel, J. Pedraza-Chaverri and L. Massieu, *Exp. Neurol.*, 2008, **211**, 85–96.

23 A. Kładna, M. Marchlewicz, T. Piechowska, I. Kruk and H. Y. Aboul-Enein, *Luminescence*, 2015, **30**, 1153–1158.

24 C. Groussard, I. Morel, M. Chevanne, M. Monnier, J. Cillard and A. Delamarche, *J. Appl. Physiol.*, 2000, **89**, 169–175.

25 M. Wollenhaupt, S. A. Carl, A. Horowitz and J. N. Crowley, *J. Phys. Chem. A*, 2000, **104**, 2695–2705.

26 Y. Zhao and D. G. Truhlar, *J. Phys. Chem. A*, 2008, **112**, 1095–1099.

27 M. D. Hanwell, D. E. Curtis, D. C. Lonie, T. Vandermeersch, E. Zurek and G. R. Hutchison, *J. Cheminf.*, 2012, **4**, 1–17.

28 (*a*) F. Neese, *Wiley Interdiscip. Rev.:Comput. Mol. Sci.*, 2022, **12**, e1606; (*b*) F. Neese, *Comput. Chem.*, 2003, **24**, 1740–1747; (*c*) F. Neese, F. Wennmohs, A. Hansen and U. Becker, *Chem. Phys.*, 2009, **356**, 98–109; (*d*) D. Bykov, T. Petrenko, R. Izsak, S. Kossmann, U. Becker, E. Valeev and F. Neese, *Mol. Phys.*, 2015, **113**, 1961–1977; (*e*) G. L. Stoychev, A. A. Auer and F. Neese, *J. Theor. Comput. Chem.*, 2017, **13**, 554–562; (*f*) M. Garcia-Rates and F. Neese, *J. Comput. Chem.*, 2019, **40**, 1816–1828; (*g*) M. Garcia-Rates and F. Neese, *J. Comput. Chem.*, 2020, **41**, 922–939; (*h*) B. Helmich-Paris de Souza, F. Neese and R. Izsák, *J. Chem. Phys.*, 2021, **155**, 104109; (*i*) F. Neese, *J. Comput. Chem.*, 2022, 1–16; (*j*) S. Grimme, J. Antony, S. Ehrlich and H. Krieg, *J. Chem. Phys.*, 2010, **132**, 154104; (*k*) R. Izsak and F. Neese, *J. Chem. Phys.*, 2011, **135**, 144105; (*l*) R. Izsak, A. Hansen and F. Neese, *Mol. Phys.*, 2012, **110**, 2413–2417; (*m*) F. Neese, *Wiley Interdiscip. Rev.:Comput. Mol. Sci.*, 2012, **2**, 73–78; (*n*) R. Izsak, F. Neese and W. Klopper, *J. Chem. Phys.*, 2013, 139; (*o*) F. Neese, *Wiley Interdiscip. Rev.:Comput. Mol. Sci.*, 2018, **8**, 1–6; (*p*) F. Neese, F. Wennmohs, U. Becker and C. Riplinger, *J. Chem. Phys.*, 2020, **152**, 224108; (*q*) F. Neese, *Chem. Phys. Lett.*, 2000, **325**, 93–98.

29 Y. Zhao, N. E. Schultz and D. G. Truhlar, *J. Chem. Theory Comput.*, 2006, **2**, 364–382.

30 Y. Zhao and D. G. Truhlar, *Theor. Chem. Acc.*, 2008, **120**, 215–241.

31 Y. Ünal, W. Nassif, B. C. Özaydin and K. Sayin, *Vib. Spectrosc.*, 2021, **112**, 103189.

32 S. Grimme, J. Antony, S. Ehrlich and H. Krieg, *J. Chem. Phys.*, 2010, **132**, 154104.

33 A. V. Marenich, C. J. Cramer and D. G. Truhlar, *J. Phys. Chem. B*, 2019, **113**, 6378–6396.

34 A. Pérez-González and A. Galano, *J. Phys. Chem. B*, 2012, **116**, 1180–1188.

35 V. Ásgeirsson, B. O. Birgisson, R. Bjornsson, U. Becker, F. Neese, C. Riplinger and H. Jónsson, *J. Chem. Theory Comput.*, 2021, **17**, 4929–4945.

36 C. Eckart, *Phys. Rev.*, 1930, **35**, 1303.

37 S. Canneaux, F. Bohr and E. Henon, *J. Comput. Chem.*, 2014, **35**, 82–93.

38 A. Fernández-Ramos, B. A. Ellingson, R. Meana-Pañeda, J. M. Marques and D. G. Truhlar, *Theor. Chem. Acc.*, 2007, **118**, 813–826.

39 S. W. Benson, *The Foundations of Chemical Kinetics*, Krieger, Florida, 1982.

40 S. R. Logan, *Fundamentals of Chemical Kinetics*, Pearson Education, London, 1996.

41 F. C. Collins and G. E. Kimball, *J. Colloid Sci.*, 1949, **4**, 425–437.

42 P. F. Stouten, L. M. Kroon-Batenburg and J. Kroon, *J. Mol. Struct.:THEOCHEM*, 1989, **200**, 169–187.

43 S. Mahmoudi, M. M. Dehkordi and M. H. Asgarshamsi, *J. Mol. Model.*, 2021, **27**, 271.

44 C. W. Mansfield, *Oxidation Reduction Potentials of Organic Systems*, Williams & Wilkins, Baltimore, USA, 1960.

45 F. A. Bulat, J. S. Murray and P. Politzer, *Comput. Theor. Chem.*, 2021, **1199**, 113192.

46 P. Sjoberg, J. S. Murray, T. Brinck and P. Politzer, *Can. J. Chem.*, 1990, **68**, 1440–1443.

47 (*a*) T. Lu and F. Chen, *J. Comput. Chem.*, 2012, **33**, 580–592; (*b*) T. Lu, *J. Chem. Phys.*, 2024, **161**, 8; (*c*) T. Lu and F. Chen, *J. Mol. Graphics Modell.*, 2012, **38**, 314–323.

48 F. Gilardoni, J. Weber, H. Chermette and T. R. Ward, *J. Phys. Chem. A*, 1998, **102**, 3607–3613.

49 A. Pérez-González and A. Galano, *J. Phys. Chem. B*, 2011, **115**, 10375–10384.

50 R. Stowasser and R. Hoffmann, *J. Am. Chem. Soc.*, 1999, **121**, 3414–3420.

51 M. Marshall, Z. Zhu, R. Harris, E. Collins and K. H. Bowen, *J. Phys. Chem. A*, 2021, **125**, 7699–7704.

52 R. V. Vedrinskii, S. A. Prosandeev and Y. A. Teterin, *Theor. Exp. Chem.*, 1981, **16**, 442–446.

53 R. A. Marcus, *Rev. Mod. Phys.*, 1993, **65**, 599–610.

54 S. F. Nelsen, S. C. Blackstock and Y. Kim, *J. Am. Chem. Soc.*, 1987, **109**, 677–682.

55 A. Galano, *J. Phys. Chem. B*, 2007, **111**, 12898–12908.

56 R. A. Marcus and N. Sutin, *Biochem. Biophys. Acta*, 1985, **811**, 265–322.

57 A. Pérez-González and A. Galano, *J. Phys. Chem. B*, 2012, **116**, 1180–1188.

58 L. Li, Y. Yao and N. Fu, *Eur. J. Org. Chem.*, 2023, e202300166.

59 A. Galano and J. R. Alvarez-Idaboy, *J. Comput. Chem.*, 2013, **34**, 2430–2445.

60 Y. Zhao, O. Tishchenko, J. R. Gour, W. Li, J. J. Lutz, P. Piecuch and D. G. Truhlar, *J. Phys. Chem. A*, 2009, **113**, 5786–5799.

61 L. M. Thompson and H. P. Hratchian, *J. Phys. Chem. A*, 2015, **119**, 8744–8751.

62 Although we use bond dissociation energies, as is common in the literature, bond dissociation free energies likely provide a more accurate evaluation of the hydrogen abstraction process. See J. J. Warren, T. A. Tronic and J. M. Mayer, *Chem. Rev.*, 2010, **110**, 6961–7001.

63 M. G. Evans and M. Polanyi, *Trans. Faraday Soc.*, 1938, **34**, 11–24.

64 T. Y. Nikolaienko and L. A. Bulavin, *Int. J. Quantum Chem.*, 2019, **119**, e25798.

65 T. Y. Nikolaienko, L. A. Bulavin and D. M. Hovorun, *Comput. Theor. Chem.*, 2014, **1050**, 15–22.

This journal is © the Owner Societies 2025

Phys. Chem. Chem. Phys., 2025, **27**, 20484–20492 | **20491**

66 A. Sirjoosingh and S. Hammes-Schiffer, *J. Phys. Chem. A*, 2011, **115**, 2367–2377.

67 L. Muñoz-Rugeles, A. Galano and J. R. Alvarez-Idaboy, *Phys. Chem. Chem. Phys.*, 2017, **19**, 6969–6972.

68 Due to the large imaginary frequency associated with this transition state, the Eckart approximation likely underestimates the tunnelling correction. More advanced methods, such as small-curvature tunnelling, could provide a more accurate evaluation; however, as we have focused on the minimum energy path connecting reactants and the transition state, this is beyond the scope of the current study.

69 J. L. Jeffrey, J. A. Terrett and D. W. MacMillan, *Science*, 2015, **349**, 1532–1536.

70 W. Sun, L. Yang, L. Yu and M. Saeys, *J. Phys. Chem. A*, 2009, **113**, 7852–7860.

71 H. P. Schuchmann and C. V. Sonntag, *Z. Naturforsch., B*, 1984, **39**, 217–221.

72 J. M. Anglada, R. Crehuet and J. S. Francisco, *Chem. – Eur. J.*, 2016, **22**, 18092–18100.

73 G. Gryn'ova and M. L. Coote, *J. Am. Chem. Soc.*, 2013, **135**, 15392–15403.

74 A. Kumar and M. D. Sevilla, *J. Phys. Chem. A*, 2018, **122**, 98–105.

75 P. Neta, M. Simic and E. Hayon, *J. Phys. Chem.*, 1969, **73**, 4207–4213.

76 J. Mandl, A. Szarka and G. Banhegyi, *Br. J. Pharmacol.*, 2009, **157**, 1097–1110.

77 B. Halliwell and J. M. C. Gutteridge, *Free Radicals in Biology & Medicine*, Oxford University Press, Oxford, UK, 5th edn, 2015.

20492 | *Phys. Chem. Chem. Phys.*, 2025, **27**, 20484–20492

This journal is © the Owner Societies 2025